Available online at www.sciencedirect.com
SCIENCE DIRECT®
Journal of Computational Physics 210 (2005) 584–607
JOURNAL OF COMPUTATIONAL PHYSICS
www.elsevier.com/locate/jcp

Artificial compressibility, characteristics-based schemes for variable density, incompressible, multi-species flows. Part I. Derivation of different formulations and constant density limit

Evgeniy Shapiro, Dimitris Drikakis *

Fluid Mechanics and Computational Science Group, School of Engineering, Cranfield University, Cranfield MK43 0AL, United Kingdom

Received 10 January 2005; received in revised form 29 April 2005; accepted 3 May 2005
Available online 11 July 2005

Abstract

The paper presents various formulations of characteristics-based schemes in the framework of the artificial-compressibility method for variable-density incompressible flows. In contrast to constant-density incompressible flows, where the characteristics-based variables *reconstruction* leads to a single formulation, in the case of variable density flows three different schemes can be obtained henceforth labeled as: *transport*, *conservative* and *hybrid* schemes. The conservative scheme results in pseudo-compressibility terms in the (multi-species) density reconstruction. It is shown that in the limit of constant density, the *transport* scheme becomes the (original) characteristics-based scheme for incompressible flows, but the *conservative* and *hybrid* schemes lead to a new characteristics-based variant for constant density flows. The characteristics-based schemes are combined with second and third-order interpolation for increasing the computational accuracy locally at the cell faces of the control volume. Numerical experiments for constant density flows reveal that all the characteristics-based schemes result in the same flow solution, but they exhibit different convergence behavior. The multigrid implementation and numerical studies for variable density flows are presented in Part II of this study.

MSC: 65C20; 76M20

Keywords: Variable density flows; Artificial compressibility; Characteristics-based schemes; High-resolution schemes; Euler equations; Navier–Stokes equations

DOI of original article: 10.1016/j.jcp.2005.05.002.
* Corresponding author. Tel.: +44 1234 754796; fax: +44 1234 758207.
E-mail address: d.drikakis@cranfield.ac.uk (D. Drikakis).

0021-9991/$ - see front matter © 2005 Elsevier Inc. All rights reserved.
doi:10.1016/j.jcp.2005.05.001

1. Introduction

The development of advanced computational models for variable density flows is motivated by several application problems including chemical reactors [1,2]; multi-material mixing [3–5]; environmental flows [6]; combustion engineering [7]; biological flow and mass transport [8]; highly stratified flows [9]; interfaces between fluid of different density [10]; inertial confinement fusion [11]; and problems in astrophysics [12]. Depending on the application, variable density flows can feature low or high speeds, a range of spatial and time scales as well as large density and temperature gradients, which in association with fast chemical reaction rates can result in stiff numerical solutions and slow convergence rates.

Another area of variable density flows is that of incompressible fluids with large (discontinuous) density variations (interfaces). Water/air free surface flow is a classical example, e.g., a water drop falling into a pool of water. Other important examples are the filling of a cast metal mold with a molten metal alloy; the production and transport of micron-sized ink drops during inkjet printer operation; as well as environmental and combustion problems. Although the present paper is not concerned with discontinuous interfaces, for completeness we mention that the variable density formulations and algorithms used in the above problems should be combined with special interface techniques such as volume tracking methods. These methods have spawned a plethora of papers including an important review [13] and extensive reference in textbooks [14], and continued development in ever more complex computational geometries. In addition to the interface tracking approach [13,15], other approaches include utilization of interface-capturing schemes (see, e.g., [16]) and hybrid approaches, e.g., [17,18].

A class of computational approaches that is frequently used for variable density problems is the pressure-projection method [19]. Bell and Marcus [20] and later on Almgren et al. [21,22] have developed second-order projection algorithms for variable-density incompressible flows. An extensive discussion of robust fractional-step projection methods for variable density flows can be found in [23]. A recent review of approximate and exact projection methods can also be found in [14]. Pressure-projection based methods have also been used in conjunction with finite-element schemes, see e.g. [24,25]; in the latter an unconditionally stable method was developed based on two projections per time step and its performance was investigated both in finite volume and finite-element implementations.

Another family of methods for solving incompressible flows is based on the artificial compressibility formulation of Chorin [26]. The artificial compressibility approach circumvents the difficulty of the pressure decoupling in the incompressible Navier–Stokes equations by adding a pseudo-time pressure derivative to the continuity equation. The new system of equations can then be iterated in pseudo-time until the divergence-free flow field is satisfied. The method can be used both for steady and unsteady flows and there are a number of papers in the literature describing implicit and explicit strategies for solving steady and unsteady flow problems in conjunction with the artificial compressibility [14,27–38]. The artificial compressibility method leads to hyperbolic and hyperbolic-parabolic equations for inviscid and viscous incompressible (constant density) flows, respectively. The discretization schemes and solvers developed for artificial compressibility have many similarities with the methods developed for compressible flows. Therefore, numerical developments for compressible flows can be transferred to incompressible flows.

Although the artificial compressibility has been used extensively for constant density flows, the development of numerical schemes in the framework of artificial compressibility for variable, density incompressible flows has received scant attention in the literature. Riedel [39] used artificial compressibility formulation to construct an unstructured finite volume method for the solution of 2-D steady viscous, incompressible, reacting flows, while Pan and Chang [40] developed a surface-capturing total variation diminishing (TVD) method with slope modification for multi-fluid incompressible Navier–Stokes formulation. Finally, Quian et al. [41] developed interface-capturing high-resolution Godunov-type scheme for hydraulic flow problems.

The aim of the present work is to develop high-resolution, characteristics-based schemes, in conjunction with the artificial compressibility approach for variable-density incompressible flows. High-resolution methods have attracted the interest of researchers in a broad range of application problems. A detailed account of the theory, numerical design practices and computational implementation of high-resolution methods for incompressible and low-speed flows can be found in [14]. These methods can provide high spatial accuracy and accurate representation of the flow physics, thus allowing accurate solutions to be obtained on moderate grids. The origin of the characteristics-based schemes derived here can be found in previous works dealt with compressible [42] and incompressible (constant density) flows [14,36]. Using the artificial compressibility framework, in the present paper we derive characteristics-based schemes for variable-density, multi-species flows.

In Part I, we present the derivation of characteristics-based schemes and assess the accuracy and efficiency of these schemes in the limit of constant-density incompressible flows. The implementation of the schemes in conjunction with multigrid acceleration techniques and numerical studies that assess the accuracy and efficiency of the schemes in variable density flows, are presented in Part II of this study.

2. Problem formulation

Constant density incompressible flows are governed by the continuity and momentum equations [14,43,44]:

$$\nabla \cdot \vec{u} = 0, \tag{1}$$

$$\frac{\partial \vec{u}}{\partial t} + (\vec{u} \cdot \nabla)\vec{u} = -\frac{1}{\rho}\nabla p + \nu \nabla^2 \vec{u}. \tag{2}$$

In the above equations, $\vec{u}$ is the velocity vector with components (u, v, w) for the three Cartesian directions (x, y, z), respectively; ρ is the fluid density; p is the pressure; and ν denotes viscosity.

For incompressible flows, the decoupling between continuity and momentum equations is due to the absence of the pressure from the former. This can be circumvented by using the artificial approach of Chorin [26], which introduces a pseudo-time pressure derivative in the continuity equation (τ is the pseudo-time),

$$\frac{1}{\beta}\frac{\partial p}{\partial \tau} + \nabla \cdot \vec{u} = 0, \tag{3}$$

where β is the artificial compressibility parameter that needs to be properly chosen in order to achieve numerical convergence. For steady state problems, (3) is solved along with the momentum equations until the pseudo-time pressure derivative vanishes. For unsteady problems a similar procedure is applied and this is discussed below.

For multispecies flows, (2) needs to be written in a form that takes into account the varying local viscosity, ν_l. Moreover, the equations can become dimensionless by introducing the local Reynolds number $Re_l = U_0 L/\nu_l$, where U_0 and L denote reference values for the velocity and spatial dimension, respectively, while ν_l is the local kinematic viscosity. One can also introduce a reference (constant) viscosity ν_0 and define the corresponding Reynolds number, based on ν_0, as $Re = Re_l \nu_l/\nu_0$. The dimensionless form of (2) is then given by

$$\frac{\partial \vec{u}}{\partial t} + (\vec{u} \cdot \nabla)\vec{u} = -\frac{1}{\rho}\nabla p + \frac{1}{Re_l}\nabla^2 \vec{u}. \tag{4}$$

Calculation of the local viscosity for a mixture of fluids may be not a trivial problem. For immiscible fluids, calculation of the local fluid properties is reduced to the determination of the interface position, which is equivalent to the solution of convection equations for fluid properties [17,45]. However, for miscible fluids local fluid properties should be computed using approximate methods (see, e.g., [46]). Alternatively, the local viscosity can be determined by a volume weighted average [47] and this is the approach followed here.

In addition to the basic fluid flow equations, for multi-species flow problems advection-diffusion equations are added to the system for tracing species propagation. The advection-diffusion equations can be casted in terms of molecular concentrations, mass fractions, mole fractions, etc. The choice of formulation depends on which representation is more convenient for each particular problem. In the present paper, we have chosen to cast the equations in terms of partial densities, ρ_i. For a flow containing N species, the total density is defined by the sum of partial densities $\rho \equiv \Sigma\rho_i$ $(i = 1, N)$. The advection-diffusion equations for species transport are given by

$$\frac{\partial\rho_i}{\partial t} + (\vec{u}\cdot\nabla)\rho_i = \frac{1}{Pe}\nabla\cdot\left(\sum_{l=1}^{l=N} D_{li}^{m}\rho\nabla\frac{\rho_l}{\rho}\right). \tag{5}$$

In the above equation, $Pe = U_0 L/D$ and $D_{li}^{m} = D_{li}^{m*}/D$ stand for the Peclet number and the normalized multi-component diffusion coefficients, respectively, where D is a reference diffusion coefficient and D_{li}^{m*} are the elements of the dimensional, multicomponent $N\times N$ diffusion matrix. In pure diffusion problems the equations for species transport (5) should be solved for all species [45]. When the flow equations are solved simultaneously with the advection-diffusion equations for species transport, it is more convenient to solve the advection equation for the total density of the flow. Because in this case the system of equations becomes overdefined – the equation for total density can be obtained as a sum of equations for partial densities – the system for species transport can be reduced to $(N-1)$ equations for partial densities ρ_i, i.e.

$$\begin{cases} \frac{\partial\rho}{\partial t} + (\vec{u}\cdot\nabla)\rho = 0, \\ \frac{\partial\rho_i}{\partial t} + (\vec{u}\cdot\nabla)\rho_i = \frac{1}{Pe}\nabla\cdot\left(\sum_{l=1}^{N-1} D_{li}\rho\nabla\frac{\rho_l}{\rho}\right), \\ i = 1,\ N-1, \end{cases} \tag{6}$$

where D_{li} are the elements of the reduced $(N-1)\times(N-1)$ matrix [48]. Generally, there is not a broadly established definition or solution for multi-component and reduced diffusion matrices apart from the dilute-gas limit [49]. In this paper, the reduced diffusion matrix is considered to be known. For a steady-state flow problem the equations to be solved are (2), (3) and (6). The artificial compressibility approach can also be used for time-dependent flow problems using the dual-time stepping technique [30,32], which results in adding a pseudo-time derivative in the momentum equations as well. For the variable-density flow case, pseudo-time density derivatives also need to be added to the species transport equations, thus yielding the following system of equations

$$\begin{cases} \frac{\partial\vec{u}}{\partial\tau} = -\frac{\partial\vec{u}}{\partial t} - ((\vec{u}\cdot\nabla)\vec{u} + \frac{1}{\rho}\nabla p - \frac{1}{Re_1}\nabla^2\vec{u}), \\ \frac{\partial p}{\partial\tau} = -\beta\nabla\cdot\vec{u}, \\ \frac{\partial\rho}{\partial\tau} = -\frac{\partial\rho}{\partial t} - (\vec{u}\cdot\nabla)\rho, \\ \frac{\partial\rho_i}{\partial\tau} = -\frac{\partial\rho_i}{\partial t} - \left((\vec{u}\cdot\nabla)\rho_i - \frac{1}{Pe}\nabla\cdot\left(\sum_{l=1}^{N-1} D_{li}\rho\nabla\frac{\rho_l}{\rho}\right)\right). \end{cases} \tag{7}$$

At each real time step, t, the solution of (7) is obtained by iterating in pseudo-time τ until convergence is achieved within a prescribed convergence tolerance; thus driving the pseudo-time derivatives to zero and satisfying the incompressibility (divergence free) condition at each real time step.

We write the system (7) in conservative form for the vector of unknown variables $\mathbf{U} = (p/\beta, \rho u, \rho v, \rho w, \rho, \rho_i)^{\mathrm{T}}$ and introduce the inviscid $(\mathbf{E_I^c}, \mathbf{F_I^c}, \mathbf{G_I^c})$ and viscous $(\mathbf{E_V^c}, \mathbf{F_V^c}, \mathbf{G_V^c})$ flux vectors for Cartesian coordinates (x, y, z):

$$\frac{\partial \mathbf{U}}{\partial \tau} = -\frac{\partial \mathbf{U_r}}{\partial t} + \frac{\partial \mathbf{E_V^c}}{\partial x} + \frac{\partial \mathbf{F_V^c}}{\partial y} + \frac{\partial \mathbf{G_V^c}}{\partial z} - \frac{\partial \mathbf{E_I^c}}{\partial x} - \frac{\partial \mathbf{F_I^c}}{\partial y} - \frac{\partial \mathbf{G_I^c}}{\partial z}, \tag{8}$$

where $\mathbf{U_r} = (0, \rho u, \rho v, \rho w, \rho, \rho_k)^{\mathrm{T}}$ and the inviscid and viscous fluxes are given by

$$\begin{cases} \mathbf{E_I^c} = (u, \rho u^2 + p, \rho uv, \rho uw, \rho u, \rho_i u)^{\mathrm{T}}, \\ \mathbf{F_I^c} = (v, \rho uv, \rho v^2 + p, \rho vw, \rho v, \rho_i v)^{\mathrm{T}}, \\ \mathbf{G_I^c} = (w, \rho uw, \rho vw, \rho w^2 + p, \rho w, \rho_i w)^{\mathrm{T}} \end{cases} \tag{9}$$

and

$$\begin{cases} \mathbf{E_V^c} = \left(0, \tau_{xx}, \tau_{xy}, \tau_{xz}, 0, \frac{1}{Pe} \sum_{l=1}^{N-1} D_{li} \rho \frac{\partial \rho_l / \rho}{\partial x}\right)^{\mathrm{T}}, \\ \mathbf{F_V^c} = \left(0, \tau_{yx}, \tau_{yy}, \tau_{yz}, 0, \frac{1}{Pe} \sum_{l=1}^{N-1} D_{li} \rho \frac{\partial \rho_l / \rho}{\partial y}\right)^{\mathrm{T}}, \\ \mathbf{G_V^c} = \left(0, \tau_{zx}, \tau_{zy}, \tau_{zz}, 0, \frac{1}{Pe} \sum_{l=1}^{N-1} D_{li} \rho \frac{\partial \rho_l / \rho}{\partial z}\right)^{\mathrm{T}}, \end{cases} \tag{10}$$

respectively, where τ_{ij} stand for the components of the viscous stress tensor. Let us consider an arbitrary curvilinear system $(\xi(x,y,z),\ \eta(x,y,z),\ \zeta(x,y,z))$ where the Jacobian of the transformation is given by $J = \left|\frac{\partial(x,y,z)}{\partial(\xi,\eta,\zeta)}\right|$. The system of (8) can be written in curvilinear coordinates (see, for example, [14]) as

$$\frac{\partial J\mathbf{U}}{\partial \tau} = -\frac{\partial J\mathbf{U_r}}{\partial t} + \frac{\partial \mathbf{E_V}}{\partial \xi} + \frac{\partial \mathbf{F_V}}{\partial \eta} + \frac{\partial \mathbf{G_V}}{\partial \zeta} - \frac{\partial \mathbf{E_I}}{\partial \xi} - \frac{\partial \mathbf{F_I}}{\partial \eta} - \frac{\partial \mathbf{G_I}}{\partial \zeta}. \tag{11}$$

The inviscid, $(\mathbf{E_I}, \mathbf{F_I}, \mathbf{G_I})$, and viscous, $(\mathbf{E_V}, \mathbf{F_V}, \mathbf{G_V})$, fluxes can be written in curvilinear coordinates as

$$\begin{cases} \mathbf{E_I} = J\left(\mathbf{E_I^c}\frac{\partial \xi}{\partial x} + \mathbf{F_I^c}\frac{\partial \xi}{\partial y} + \mathbf{G_I^c}\frac{\partial \xi}{\partial z}\right), \\ \mathbf{F_I} = J\left(\mathbf{E_I^c}\frac{\partial \eta}{\partial x} + \mathbf{F_I^c}\frac{\partial \eta}{\partial y} + \mathbf{G_I^c}\frac{\partial \eta}{\partial z}\right), \\ \mathbf{G_I} = J\left(\mathbf{E_I^c}\frac{\partial \zeta}{\partial x} + \mathbf{F_I^c}\frac{\partial \zeta}{\partial y} + \mathbf{G_I^c}\frac{\partial \zeta}{\partial z}\right), \\ \mathbf{E_V} = J\left(\mathbf{E_V^c}\frac{\partial \xi}{\partial x} + \mathbf{F_V^c}\frac{\partial \xi}{\partial y} + \mathbf{G_V^c}\frac{\partial \xi}{\partial z}\right), \\ \mathbf{F_V} = J\left(\mathbf{E_V^c}\frac{\partial \eta}{\partial x} + \mathbf{F_V^c}\frac{\partial \eta}{\partial y} + \mathbf{G_V^c}\frac{\partial \eta}{\partial z}\right), \\ \mathbf{G_V} = J\left(\mathbf{E_V^c}\frac{\partial \zeta}{\partial x} + \mathbf{F_V^c}\frac{\partial \zeta}{\partial y} + \mathbf{G_V^c}\frac{\partial \zeta}{\partial z}\right). \end{cases} \tag{12}$$

Using the above notation, in the next section we present the derivation of characteristics-based schemes for variable-density incompressible flows.

3. Characteristics-based schemes

Both the advective and viscous fluxes are discretized on the cell centres using the intercell values (Fig. 1), e.g.,

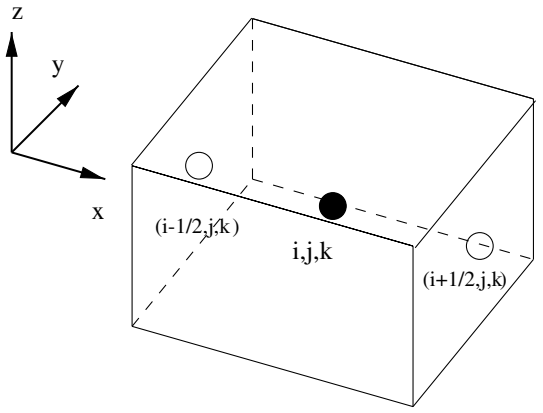

Fig. 1. Computational cell notation.

$$\frac{\partial \mathbf{E_I}}{\partial \xi} = \frac{(\mathbf{E_I})_{i+\frac{1}{2},j,k} - (\mathbf{E_I})_{i-\frac{1}{2},j,k}}{\Delta \xi}. \tag{13}$$

Let us consider (11) retaining only the inviscid part of the operator and omitting the derivative in real time. The latter can be treated as a source term without affecting the derivation of the characteristics-based scheme. Then (11) is written

$$\begin{aligned}
\frac{\partial J\mathbf{U}}{\partial \tau} + \frac{\partial \mathbf{E_I}}{\partial \xi} + \frac{\partial \mathbf{F_I}}{\partial \eta} + \frac{\partial \mathbf{G_I}}{\partial \zeta} &= \frac{\partial J\mathbf{U}}{\partial \tau} + \frac{\partial J\left(\mathbf{E_I^c}\frac{\partial \xi}{\partial x} + \mathbf{F_I^c}\frac{\partial \xi}{\partial y} + \mathbf{G_I^c}\frac{\partial \xi}{\partial z}\right)}{\partial \xi} + \frac{\partial J\left(\mathbf{E_I^c}\frac{\partial \eta}{\partial x} + \mathbf{F_I^c}\frac{\partial \eta}{\partial y} + \mathbf{G_I^c}\frac{\partial \eta}{\partial z}\right)}{\partial \eta} \\
&\quad + \frac{\partial J\left(\mathbf{E_I^c}\frac{\partial \zeta}{\partial x} + \mathbf{F_I^c}\frac{\partial \zeta}{\partial y} + \mathbf{G_I^c}\frac{\partial \zeta}{\partial z}\right)}{\partial \zeta} \\
&= J\frac{\partial \mathbf{U}}{\partial \tau} + J\left(\frac{\partial \xi}{\partial x}\frac{\partial \mathbf{E_I^c}}{\partial \xi} + \frac{\partial \xi}{\partial y}\frac{\partial \mathbf{F_I^c}}{\partial \xi} + \frac{\partial \xi}{\partial z}\frac{\partial \mathbf{G_I^c}}{\partial \xi}\right) + J\left(\frac{\partial \eta}{\partial x}\frac{\partial \mathbf{E_I^c}}{\partial \eta} + \frac{\partial \eta}{\partial y}\frac{\partial \mathbf{F_I^c}}{\partial \eta} + \frac{\partial \eta}{\partial z}\frac{\partial \mathbf{G_I^c}}{\partial \eta}\right) \\
&\quad + J\left(\frac{\partial \eta}{\partial x}\frac{\partial \mathbf{E_I^c}}{\partial \eta} + \frac{\partial \eta}{\partial y}\frac{\partial \mathbf{F_I^c}}{\partial \eta} + \frac{\partial \eta}{\partial z}\frac{\partial \mathbf{G_I^c}}{\partial \eta}\right) + \mathbf{E_I^c}\left(\frac{\partial}{\partial \xi}\left(J\frac{\partial \xi}{\partial x}\right) + \frac{\partial}{\partial \eta}\left(J\frac{\partial \eta}{\partial x}\right) + \frac{\partial}{\partial \zeta}\left(J\frac{\partial \zeta}{\partial x}\right)\right) \\
&\quad + \mathbf{F_I^c}\left(\frac{\partial}{\partial \xi}\left(J\frac{\partial \xi}{\partial y}\right) + \frac{\partial}{\partial \eta}\left(J\frac{\partial \eta}{\partial y}\right) + \frac{\partial}{\partial \zeta}\left(J\frac{\partial \zeta}{\partial y}\right)\right) \\
&\quad + \mathbf{G_I^c}\left(\frac{\partial}{\partial \xi}\left(J\frac{\partial \xi}{\partial z}\right) + \frac{\partial}{\partial \eta}\left(J\frac{\partial \eta}{\partial z}\right) + \frac{\partial}{\partial \zeta}\left(J\frac{\partial \zeta}{\partial z}\right)\right),
\end{aligned} \tag{14}$$

where the brackets in the last three terms are zero (this can be shown by substituting the expression for the Jacobian into the brackets and performing differentiation). We consider the one-dimensional counterpart of (14), with respect to the ξ-direction (for non-moving grids),

$$\frac{\partial \mathbf{U}}{\partial \tau} + \frac{\partial \xi}{\partial x}\frac{\partial \mathbf{E_I^c}}{\partial \xi} + \frac{\partial \xi}{\partial y}\frac{\partial \mathbf{F_I^c}}{\partial \xi} + \frac{\partial \xi}{\partial z}\frac{\partial \mathbf{G_I^c}}{\partial \xi} = 0, \tag{15}$$

divide by $\sqrt{\left(\frac{\partial \xi}{\partial x}\right)^2 + \left(\frac{\partial \xi}{\partial y}\right)^2 + \left(\frac{\partial \xi}{\partial z}\right)^2}$ and introduce the notation

$$L = \sqrt{\left(\frac{\partial \xi}{\partial x}\right)^2 + \left(\frac{\partial \xi}{\partial y}\right)^2 + \left(\frac{\partial \xi}{\partial z}\right)^2} \tag{16}$$

and $\tilde{k} = \frac{1}{L}\frac{\partial \xi}{\partial k}$, where $k = x, y, z$. Eq. (15) can then be written as a system of equations

$$\begin{cases} \frac{1}{\beta L}\frac{\partial p}{\partial \tau} + \tilde{x}\frac{\partial u}{\partial \xi} + \tilde{y}\frac{\partial v}{\partial \xi} + \tilde{z}\frac{\partial w}{\partial \xi} = 0, \\ \frac{1}{L}\frac{\partial (\rho u)}{\partial \tau} + \tilde{x}\frac{\partial (\rho u^2 + p)}{\partial \xi} + \tilde{y}\frac{\partial (\rho uv)}{\partial \xi} + \tilde{z}\frac{\partial (\rho uw)}{\partial \xi} = 0, \\ \frac{1}{L}\frac{\partial (\rho v)}{\partial \tau} + \tilde{x}\frac{\partial (\rho uv)}{\partial \xi} + \tilde{y}\frac{\partial (\rho v^2 + p)}{\partial \xi} + \tilde{z}\frac{\partial (\rho vw)}{\partial \xi} = 0, \\ \frac{1}{L}\frac{\partial (\rho w)}{\partial \tau} + \tilde{x}\frac{\partial (\rho uw)}{\partial \xi} + \tilde{y}\frac{\partial (\rho vw)}{\partial \xi} + \tilde{z}\frac{\partial (\rho w^2 + p)}{\partial \xi} = 0, \\ \frac{1}{L}\frac{\partial \rho}{\partial \tau} + \tilde{x}\frac{\partial (\rho u)}{\partial \xi} + \tilde{y}\frac{\partial (\rho v)}{\partial \xi} + \tilde{z}\frac{\partial (\rho w)}{\partial \xi} = 0, \\ \frac{1}{L}\frac{\partial \rho_i}{\partial \tau} + \tilde{x}\frac{\partial (\rho_i u)}{\partial \xi} + \tilde{y}\frac{\partial (\rho_i v)}{\partial \xi} + \tilde{z}\frac{\partial (\rho_i w)}{\partial \xi} = 0, \\ i = 1, \ N - 1. \end{cases} \tag{17}$$

Eqs. (17) do not correspond to the system comprising of (1), (4) and (6) or (7) based on the artificial compressibility formulation – unless we apply the divergence-free condition. For example, applying the divergence-free condition to the density equations, we obtain the non-conservative form

$$\begin{cases} \frac{1}{L}\frac{\partial \rho}{\partial \tau} + (u\tilde{x} + v\tilde{y} + w\tilde{z})\frac{\partial \rho}{\partial \xi} = 0, \\ \frac{1}{L}\frac{\partial \rho_i}{\partial \tau} + (u\tilde{x} + v\tilde{y} + w\tilde{z})\frac{\partial \rho_i}{\partial \xi} = 0, \\ i = 1, \ N - 1, \end{cases} \tag{18}$$

which represents advection of density along streamlines. Eqs. (17) contain 'non-physical' terms that are divergence-velocity dependent and arise from the implementation of the artificial compressibility approach, while Eqs. (18) correspond to (6) or (7) after implementing artificial-compressibility. Through proper combinations of (17) and (18), one can derive three different formulations for Eqs. (17), which in turn lead to different characteristics-based discretizations as we will present later. The three formulations are:

Transport formulation: The equations for densities are written as advection equations in non-conservative form (18) and these are, subsequently, used to eliminate the total density from the momentum equations (17).
Hybrid formulation: The conservative equation for the total density is used to eliminate density from the momentum equations in (17). The latter are solved in conjunction with advection equations for species transport (18).
Conservative formulation: Eqs. (17) are solved without taking into account (18).

The above three formulations converge to the same system of equations as the divergence of velocity tends to zero, but they yield different characteristics-based (CB) schemes. The derivation of these schemes is discussed below.

3.1. Transport CB scheme

The transport formulation leads to the following non-conservative system of equations:

$$\begin{cases} \frac{1}{\beta L}\frac{\partial p}{\partial \tau}+\tilde{x}\frac{\partial u}{\partial \xi}+\tilde{y}\frac{\partial v}{\partial \xi}+\tilde{z}\frac{\partial w}{\partial \xi}=0, \\ \frac{1}{L}\frac{\partial u}{\partial \tau}+(u\tilde{x}+v\tilde{y}+w\tilde{z})\frac{\partial u}{\partial \xi}+(\tilde{x}\frac{\partial u}{\partial \xi}+\tilde{y}\frac{\partial v}{\partial \xi}+\tilde{z}\frac{\partial w}{\partial \xi})u+\frac{1}{\rho}\frac{\partial p}{\partial \xi}\tilde{x}=0, \\ \frac{1}{L}\frac{\partial v}{\partial \tau}+(u\tilde{x}+v\tilde{y}+w\tilde{z})\frac{\partial v}{\partial \xi}+(\tilde{x}\frac{\partial u}{\partial \xi}+\tilde{y}\frac{\partial v}{\partial \xi}+\tilde{z}\frac{\partial w}{\partial \xi})v+\frac{1}{\rho}\frac{\partial p}{\partial \xi}\tilde{y}=0, \\ \frac{1}{L}\frac{\partial w}{\partial \tau}+(u\tilde{x}+v\tilde{y}+w\tilde{z})\frac{\partial w}{\partial \xi}+(\tilde{x}\frac{\partial u}{\partial \xi}+\tilde{y}\frac{\partial v}{\partial \xi}+\tilde{z}\frac{\partial w}{\partial \xi})w+\frac{1}{\rho}\frac{\partial p}{\partial \xi}\tilde{z}=0, \\ \frac{1}{L}\frac{\partial \rho}{\partial \tau}+(u\tilde{x}+v\tilde{y}+w\tilde{z})\frac{\partial \rho}{\partial \xi}=0, \\ \frac{1}{L}\frac{\partial \rho_i}{\partial \tau}+(u\tilde{x}+v\tilde{y}+w\tilde{z})\frac{\partial \rho_i}{\partial \xi}=0, \\ i=1,\ N-1. \end{cases} \tag{19}$$

Introducing the vector of non-conservative variables, $\mathbf{U}^{\mathrm{nc}}=(\frac{p}{\beta},u,v,w,\rho,\rho_i)$, (19) can be written in a matrix form

$$\frac{1}{L}\frac{\partial \mathbf{U}^{\mathrm{nc}}}{\partial \tau}+\mathbf{A}\frac{\partial \mathbf{U}^{\mathrm{nc}}}{\partial \xi}=0, \tag{20}$$

where $\mathbf{A}$, $(4+N)\times(4+N)$, is given by

$$\mathbf{A}=\begin{pmatrix} 0 & \beta\tilde{x} & \beta\tilde{y} & \beta\tilde{z} & 0 & 0 & \dots & 0 \\ \frac{1}{\rho}\tilde{x} & \lambda_0+u\tilde{x} & u\tilde{y} & u\tilde{z} & 0 & 0 & \dots & 0 \\ \frac{1}{\rho}\tilde{y} & v\tilde{x} & \lambda_0+v\tilde{y} & v\tilde{z} & 0 & 0 & \dots & 0 \\ \frac{1}{\rho}\tilde{z} & w\tilde{x} & w\tilde{y} & \lambda_0+w\tilde{z} & 0 & 0 & \dots & 0 \\ 0 & 0 & 0 & 0 & \lambda_0 & 0 & \dots & 0 \\ 0 & 0 & 0 & 0 & 0 & \lambda_0 & \dots & 0 \\ . & . & . & . & . & . & \dots & . \\ 0 & 0 & 0 & 0 & 0 & 0 & \dots & \lambda_0 \end{pmatrix}, \tag{21}$$

with the columns and rows from 6 to $N+4$ corresponding to the species densities.

The matrix $\mathbf{A}$ has the following distinct eigenvalues: $N+2$ eigenvalues $\lambda_0=u\tilde{x}+v\tilde{y}+w\tilde{z}$ and the eigenvalues $\lambda_1=\lambda_0+s$ and $\lambda_2=\lambda_0-s$, where $s=\sqrt{\lambda_0^2+\beta/\rho}$ is the artificial speed of sound. Our objective is to derive solutions for the primitive variables along the characteristics $l=0,1,2$. Defining the characteristic directions by $\frac{\Delta\xi}{\Delta\tau}=\frac{\xi-\xi_l}{\Delta\tau}=\lambda_l\sqrt{\xi_x^2+\xi_y^2+\xi_z^2}$, the pseudo-time derivatives in (19) can be discretized as follows

$$\begin{aligned} \frac{\partial f(\tau,\xi)}{\partial \tau} &\cong \frac{f(\tau+\Delta\tau,\xi)-f(\tau,\xi)}{\Delta\tau}=\frac{f(\tau+\Delta\tau,\xi)-f(\tau,\xi_l)}{\Delta\tau}+\frac{f(\tau,\xi_l)-f(\tau,\xi)}{\Delta\tau} \\ &=\frac{f(\tau+\Delta\tau,\xi)-f(\tau,\xi_l)}{\Delta\tau}-\frac{\Delta\xi}{\Delta\tau}\frac{f(\tau,\xi_l)-f(\tau,\xi)}{\Delta\xi} \\ &=\frac{f(\tau+\Delta\tau,\xi)-f(\tau,\xi_l)}{\Delta\tau}-\frac{f(\tau,\xi_l)-f(\tau,\xi)}{\Delta\xi}\lambda\sqrt{\xi_x^2+\xi_y^2+\xi_z^2} \\ &\cong \frac{f(\tau+\Delta\tau,\xi)-f(\tau,\xi_l)}{\Delta\tau}-\frac{\partial f}{\partial \xi}\lambda\sqrt{\xi_x^2+\xi_y^2+\xi_z^2}=\frac{\tilde{f}-f}{\Delta\tau}-\frac{\partial f}{\partial \xi}\lambda\sqrt{\xi_x^2+\xi_y^2+\xi_z^2}, \end{aligned} \tag{22}$$

where $\tilde{f}\equiv f(\tau+\Delta\tau,\xi)$ and $f\equiv f(\tau,\xi_l)$ (see Fig. 2). Using (22), (19) is written:

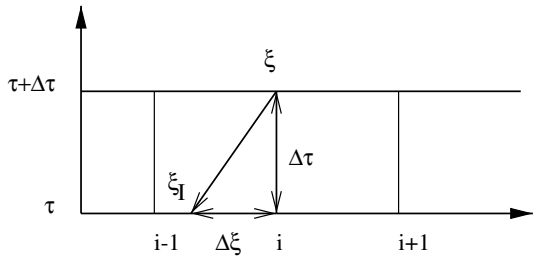

Fig. 2. Schematic of characteristics-based discretization.

$$\begin{cases} \frac{1}{\beta L}\frac{\tilde{p}-p_l}{\Delta\tau} - \frac{\lambda}{\beta}p_\xi + \tilde{x}\frac{\partial u}{\partial\xi} + \tilde{y}\frac{\partial v}{\partial\xi} + \tilde{z}\frac{\partial w}{\partial\xi} = 0, \\ \frac{1}{L}\frac{\tilde{u}-u_l}{\Delta\tau} + (\lambda_0-\lambda)\frac{\partial u}{\partial\xi} + (\tilde{x}\frac{\partial u}{\partial\xi} + \tilde{y}\frac{\partial v}{\partial\xi} + \tilde{z}\frac{\partial w}{\partial\xi})u + \frac{1}{\rho}\frac{\partial p}{\partial\xi}\tilde{x} = 0, \\ \frac{1}{L}\frac{\tilde{v}-v_l}{\Delta\tau} + (\lambda_0-\lambda)\frac{\partial v}{\partial\xi} + (\tilde{x}\frac{\partial u}{\partial\xi} + \tilde{y}\frac{\partial v}{\partial\xi} + \tilde{z}\frac{\partial w}{\partial\xi})v + \frac{1}{\rho}\frac{\partial p}{\partial\xi}\tilde{y} = 0, \\ \frac{1}{L}\frac{\tilde{w}-w_l}{\Delta\tau} + (\lambda_0-\lambda)\frac{\partial w}{\partial\xi} + (\tilde{x}\frac{\partial u}{\partial\xi} + \tilde{y}\frac{\partial v}{\partial\xi} + \tilde{z}\frac{\partial w}{\partial\xi})w + \frac{1}{\rho}\frac{\partial p}{\partial\xi}\tilde{z} = 0, \\ \frac{1}{L}\frac{\tilde{\rho}-\rho_l}{\Delta\tau} + (\lambda_0-\lambda)\frac{\partial\rho}{\partial\xi} = 0, \\ \frac{1}{L}\frac{\tilde{\rho}_i-\rho_{il}}{\Delta\tau} + (\lambda_0-\lambda)\frac{\partial\rho_i}{\partial\xi} = 0, \\ i = 1,\ N-1. \end{cases} \tag{23}$$

To eliminate the spatial derivatives from (23) we make use of the idea presented in the book of Courant and Hilbert [50] regarding elimination of unknowns in a system of linear equations, known as Riemann method. According to [50], one can multiply each from the equations in (23) with arbitrary coefficients $(a, b, c, d, e, f_i, i = 1, N-1)$, sum up the equations, group the multipliers of spatial derivatives and set them equal to zero, thus yielding the following system of equations:

$$\begin{cases} \frac{a}{\beta}(\tilde{p}-p_l) + b(\tilde{u}-u_l) + c(\tilde{v}-v_l) + d(\tilde{w}-w_l) + e(\tilde{\rho}-\rho_l) + \sum_{i=1}^{N-1} f_i(\tilde{\rho}_i-\rho_{il}) = 0, \\ -a\frac{\rho}{\beta}\lambda_l + b\tilde{x} + c\tilde{y} + d\tilde{z} = 0, \\ a\tilde{x} + b(\lambda_0-\lambda_l+u\tilde{x}) + cv\tilde{x} + dw\tilde{x} = 0, \\ a\tilde{y} + bu\tilde{y} + c(\lambda_0-\lambda_l+v\tilde{y}) + dw\tilde{y} = 0, \\ a\tilde{z} + bu\tilde{z} + cv\tilde{z} + d(\lambda_0-\lambda_l+w\tilde{z}) = 0, \\ e(\lambda_0-\lambda_l) = 0, \\ f_i(\lambda_0-\lambda_l) = 0, \\ i = 1,\ N-1, \end{cases} \tag{24}$$

where the subscript l stands for the characteristics. For $\lambda = \lambda_0$, (24) yields

$$\begin{cases} \frac{a}{\beta}(\tilde{p}-p_0) + b(\tilde{u}-u_0) + c(\tilde{v}-v_0) + d(\tilde{w}-w_0) + e(\tilde{\rho}-\rho_0) + \sum_{i=1}^{N-1} f_i(\tilde{\rho}_i-\rho_{i0}) = 0, \\ -a\frac{\rho}{\beta}\lambda_0 + b\tilde{x} + c\tilde{y} + d\tilde{z} = 0, \\ a + bu + cv + dw = 0, \\ e\cdot 0 = 0, \\ f_i\cdot 0 = 0, \\ i = 1,\ N-1, \end{cases} \tag{25}$$

The coefficients e and f_i can take any values that satisfy the last two equations in (25) and $\forall i$. Thus, from the first equation in the above system we obtain $\rho = \rho_0$ and $\rho_i = \rho_{i0}$. Taking into account that λ_0 corresponds to a streamline, we can write that $\tilde{x}v_0 - \tilde{y}u_0 = \tilde{z}u_0 - \tilde{x}w_0 = 0$, i.e., vorticity is zero along the streamline. The above yields the following system

$$\begin{cases} (\tilde{v} - v_0)\tilde{x} - (u - u_0)\tilde{y} = 0, \\ (\tilde{w} - w_0)\tilde{x} - (u - u_0)\tilde{z} = 0, \\ \rho - \rho_0 = 0, \\ \rho_i - \rho_{i0} = 0, \\ i = 1,\ N - 1. \end{cases} \tag{26}$$

For $\lambda = \lambda_1 = \lambda_0 + s$ it follows from the last two equations of (24) that $e = f_i = 0$, thus the system is written as:

$$\begin{cases} \frac{1}{\beta}(\tilde{p} - p_1) + \frac{b}{a}(\tilde{u} - u_1) + \frac{c}{a}(\tilde{v} - v_1) + \frac{d}{a}(\tilde{w} - w_1) = 0, \\ -a\frac{\rho}{\beta}(\lambda_0 + s) + b\tilde{x} + c\tilde{y} + d\tilde{z} = 0, \\ a\tilde{x} + b(-s + u\tilde{x}) + cv\tilde{x} + dw\tilde{x} = 0, \\ a\tilde{y} + bu\tilde{y} + c(-s + v\tilde{y}) + dw\tilde{y} = 0, \\ a\tilde{z} + bu\tilde{z} + cv\tilde{z} + d(-s + w\tilde{z}) = 0. \end{cases} \tag{27}$$

This system is essentially the same as for the incompressible (constant density) flow [14,36] and its solution for p is given by

$$\tilde{p} = p_1 - \rho\lambda_1[\tilde{x}(\tilde{u} - u_1) + \tilde{y}(\tilde{v} - v_1) + \tilde{z}(\tilde{w} - w_1)]. \tag{28}$$

Similarly, for $\lambda = \lambda_1 = \lambda_0 + s$ one obtains:

$$\tilde{p} = p_2 - \rho\lambda_2[\tilde{x}(\tilde{u} - u_2) + \tilde{y}(\tilde{v} - v_2) + \tilde{z}(\tilde{w} - w_2)]. \tag{29}$$

The solution of the system (26), (28) and (29) yields the following formulas for the reconstructed (tilde) variables:

$$\begin{cases} \tilde{p} = \frac{1}{2s}(\lambda_1 p_2 - \lambda_2 p_1 - \beta(R_1 - R_2)), \\ \tilde{u} = u_0 + \frac{\tilde{x}}{2s\rho}R_3, \\ \tilde{v} = v_0 + \frac{\tilde{y}}{2s\rho}R_3, \\ \tilde{w} = w_0 + \frac{\tilde{z}}{2s\rho}R_3, \\ \tilde{\rho} = \rho_0, \\ \tilde{\rho}_i = \rho_{i0}, \\ i = 1,\ N - 1. \end{cases} \tag{30}$$

In (30) we have introduced the auxiliary functions R_1, R_2 and R_3, which are given by

$$\begin{cases} R_1 = \tilde{x}(u_0 - u_1) + \tilde{y}(v_0 - v_1) + \tilde{z}(w_0 - w_1), \\ R_2 = \tilde{x}(u_0 - u_2) + \tilde{y}(v_0 - v_2) + \tilde{z}(w_0 - w_2), \\ R_3 = p_1 - p_2 + \lambda_2\rho R_2 - \lambda_1\rho R_1. \end{cases} \tag{31}$$

In the limit of constant-density flow, the eigenvalues and the reconstruction formulas for the *transport* CB scheme (30) correspond to the formulas obtained for incompressible, constant-density flows [14,36].

3.2. Hybrid CB scheme

The hybrid formulation leads to the following system of equations (with respect to the flux $\mathbf{E_I}$):

$$\begin{cases} \frac{1}{\beta L}\frac{\partial p}{\partial \tau}+\tilde{x}\frac{\partial u}{\partial \xi}+\tilde{y}\frac{\partial v}{\partial \xi}+\tilde{z}\frac{\partial w}{\partial \xi}=0, \\ \frac{1}{L}\frac{\partial u}{\partial \tau}+(u\tilde{x}+v\tilde{y}+w\tilde{z})\frac{\partial u}{\partial \xi}+\frac{1}{\rho}\frac{\partial p}{\partial \xi}\tilde{x}=0, \\ \frac{1}{L}\frac{\partial v}{\partial \tau}+(u\tilde{x}+v\tilde{y}+w\tilde{z})\frac{\partial v}{\partial \xi}+\frac{1}{\rho}\frac{\partial p}{\partial \xi}\tilde{y}=0, \\ \frac{1}{L}\frac{\partial w}{\partial \tau}+(u\tilde{x}+v\tilde{y}+w\tilde{z})\frac{\partial w}{\partial \xi}+\frac{1}{\rho}\frac{\partial p}{\partial \xi}\tilde{z}=0, \\ \frac{1}{L}\frac{\partial \rho}{\partial \tau}+(u\tilde{x}+v\tilde{y}+w\tilde{z})\frac{\partial \rho}{\partial \xi}=0, \\ \frac{1}{L}\frac{\partial \rho_i}{\partial \tau}+(u\tilde{x}+v\tilde{y}+w\tilde{z})\frac{\partial \rho_i}{\partial \xi}=0, \\ i=1,\ N-1, \end{cases} \tag{32}$$

The system (32) can be written in the matrix form (20), where $\mathbf{A}$, $(4+N)\times(4+N)$, is given by:

$$\mathbf{A}=\begin{pmatrix} 0 & \beta\tilde{x} & \beta\tilde{y} & \beta\tilde{z} & 0 & 0 & \dots & 0 \\ \frac{1}{\rho}\tilde{x} & \lambda_0 & 0 & 0 & 0 & 0 & \dots & 0 \\ \frac{1}{\rho}\tilde{y} & 0 & \lambda_0 & 0 & 0 & 0 & \dots & 0 \\ \frac{1}{\rho}\tilde{z} & 0 & 0 & \lambda_0 & 0 & 0 & \dots & 0 \\ 0 & 0 & 0 & 0 & \lambda_0 & 0 & \dots & 0 \\ 0 & 0 & 0 & 0 & 0 & \lambda_0 & \dots & 0 \\ . & . & . & . & . & . & \dots & . \\ 0 & 0 & 0 & 0 & 0 & . & \dots & \lambda_0 \end{pmatrix}. \tag{33}$$

The matrix $\mathbf{A}$ has $N+2$ eigenvalues λ_0 and the eigenvalues $\lambda_1=(\lambda_0+s)/2$, $\lambda_2=(\lambda_0-s)/2$, where the artificial speed of sound is given by $s=\sqrt{\lambda_0^2+4\frac{\beta}{\rho}}$. Application of the Riemann method for the system (32) yields,

$$\begin{cases} a\frac{1}{\beta}(\tilde{p}-p_l)+b(\tilde{u}-u_l)+c(\tilde{v}-v_l)+d(\tilde{w}-w_l)+e(\tilde{\rho}-\rho_l)+\sum_{i=1}^{N-1}f_i(\tilde{\rho}_i-\rho_{il})=0, \\ a\tilde{x}+b(\lambda_0-\lambda_l)=0, \\ a\tilde{y}+c(\lambda_0-\lambda_l)=0, \\ a\tilde{z}+d(\lambda_0-\lambda_l)=0, \\ e(\lambda_0-\lambda_l)=0, \\ f_i(\lambda_0-\lambda_l)=0, \\ i=1,\ N-1, \end{cases} \tag{34}$$

where the subscript l stands for the characteristics. When $\lambda=\lambda_0$, (34) yields,

$$\begin{cases} a\frac{1}{\beta}(\tilde{p}-p_l)+b(\tilde{u}-u_l)+c(\tilde{v}-v_l)+d(\tilde{w}-w_l)+e(\tilde{\rho}-\rho_l)+\sum_{i=1}^{N-1} f_i(\tilde{\rho}_i-\rho_{il})=0,\\ -a\frac{\rho}{\beta}\lambda_0+b\tilde{x}+c\tilde{y}+d\tilde{z}=0,\\ a\tilde{x}=0,\\ a\tilde{y}=0,\\ a\tilde{z}=0,\\ e\cdot 0=0,\\ f_i\cdot 0=0,\\ i=1,\ N-1. \end{cases} \tag{35}$$

Similarly to the *transport* scheme, in the present case $\tilde{\rho}=\rho_0$ and $\tilde{\rho}_i=\rho_{i0}$. Also (35) gives $a=0$, thus from the second equation of the above system we obtain $b=-(c\tilde{y}+d\tilde{z})/\tilde{x}$. Substituting the results into the first equation, consolidating the coefficients and setting their multipliers equal to zero, we obtain:

$$\begin{cases} (\tilde{v}-v_0)\tilde{x}-(\tilde{u}-u_0)\tilde{y}=0,\\ (\tilde{w}-w_0)\tilde{x}-(\tilde{u}-u_0)\tilde{z}=0. \end{cases} \tag{36}$$

When $\lambda=\lambda_1=(\lambda_0+s)/2$, one obtains $\lambda_0-\lambda_1=\lambda_2$ and

$$\begin{cases} \frac{a}{\beta}(\tilde{p}-p_1)+b(\tilde{u}-u_1)+c(\tilde{v}-v_1)+d(\tilde{w}-w_1)+e(\tilde{\rho}-\rho_1)+\sum_{i=1}^{N-1} f_i(\tilde{\rho}_i-\rho_{i1})=0,\\ -a\frac{\rho}{\beta}\lambda_1+b\tilde{x}+c\tilde{y}+d\tilde{z}=0,\\ a\tilde{x}+b\lambda_2=0,\\ a\tilde{y}+c\lambda_2=0,\\ a\tilde{z}+d\lambda_2=0,\\ e\lambda_2=0,\\ f_i\lambda_2=0,\\ i=1,\ N-1, \end{cases} \tag{37}$$

which yields $e=0$ and $f_i=0$, thus leading to the following system,

$$\begin{cases} a\frac{1}{\beta}(\tilde{p}-p_1)+b(\tilde{u}-u_1)+c(\tilde{v}-v_1)+d(\tilde{w}-w_1)=0,\\ -a\frac{\rho}{\beta}\lambda_1+b\tilde{x}+c\tilde{y}+d\tilde{z}=0,\\ -\frac{\tilde{x}}{\lambda_2}a=b,\\ -\frac{\tilde{y}}{\lambda_2}a=c,\\ -\frac{\tilde{z}}{\lambda_2}a=d. \end{cases} \tag{38}$$

Substituting the expressions for the coefficients b, c and d from the last three equations into the second equation and taking into account that $\tilde{x}^2+\tilde{y}^2+\tilde{z}^2=1$ and $\lambda_1\lambda_2=-\beta/\rho$, we find that the second equation in (38) becomes an identity. Substituting the expressions for the coefficients b, c and d into the first equation one obtains:

$$a\frac{1}{\beta}(\tilde{p}-p_1)-a\frac{\tilde{x}}{\lambda_2}(\tilde{u}-u_1)-a\frac{\tilde{y}}{\lambda_2}(\tilde{v}-v_1)-a\frac{\tilde{z}}{\lambda_2}(\tilde{w}-w_1)=0, \tag{39}$$

which yields that either we have a solution identical to zero for all the coefficients or

$$\tilde{p} - p_1 - \frac{\beta\tilde{x}}{\lambda_2}(\tilde{u} - u_1) - \frac{\beta\tilde{y}}{\lambda_2}(\tilde{v} - v_1) - \frac{\beta\tilde{z}}{\lambda_2}(\tilde{w} - w_1) = 0. \tag{40}$$

Since $\lambda_2\lambda_1 = -\frac{\beta}{\rho}$, the last equation can be written as

$$\tilde{p} - p_1 + \lambda_1\rho\tilde{x}(\tilde{u} - u_1) + \lambda_1\rho\tilde{y}(\tilde{v} - v_1) + \lambda_1\rho\tilde{z}(\tilde{w} - w_1) = 0. \tag{41}$$

Similarly, when $\lambda = \lambda_2 = (\lambda_0 - s)/2$ we obtain $\lambda_0 - \lambda_2 = \lambda_1$ and

$$\tilde{p} - p_2 + \lambda_2\rho\tilde{x}(\tilde{u} - u_2) + \lambda_2\rho\tilde{y}(\tilde{v} - v_2) + \lambda_2\rho\tilde{z}(\tilde{w} - w_2) = 0. \tag{42}$$

Eqs. (36), (41) and (42) lead to the following solution for the characteristics-based variables,

$$\begin{cases} \tilde{p} = \frac{1}{s}(\lambda_1 p_2 - \lambda_2 p_1 - \beta(R_1 - R_2)), \\ \tilde{u} = u_0 + \frac{\tilde{x}}{s\rho}R_3, \\ \tilde{v} = v_0 + \frac{\tilde{y}}{s\rho}R_3, \\ \tilde{w} = w_0 + \frac{\tilde{z}}{s\rho}R_3, \\ \tilde{\rho} = \rho_0, \\ \tilde{\rho}_i = \rho_{i0}, \end{cases} \tag{43}$$

where the auxiliary functions R_1, R_2 and R_3 are defined by (31). Similarly to the *transport* scheme, in the *hybrid* schemes the densities take the form of (passive) advected scalars. However, the eigenvalues as well as the formulas for the characteristics-based pressure and velocities (tilde variables) are different.

3.3. Conservative CB scheme

We consider the system (17) and write it in the form

$$\begin{cases} \frac{1}{\beta L}\frac{\partial p}{\partial \tau} + \tilde{x}\frac{\partial u}{\partial \xi} + \tilde{y}\frac{\partial v}{\partial \xi} + \tilde{z}\frac{\partial w}{\partial \xi} = 0, \\ \frac{1}{L}\frac{\partial u}{\partial \tau} + (u\tilde{x} + v\tilde{y} + w\tilde{z})\frac{\partial u}{\partial \xi} + \frac{1}{\rho}\frac{\partial p}{\partial \xi}\tilde{x} = 0, \\ \frac{1}{L}\frac{\partial v}{\partial \tau} + (u\tilde{x} + v\tilde{y} + w\tilde{z})\frac{\partial v}{\partial \xi} + \frac{1}{\rho}\frac{\partial p}{\partial \xi}\tilde{y} = 0, \\ \frac{1}{L}\frac{\partial w}{\partial \tau} + (u\tilde{x} + v\tilde{y} + w\tilde{z})\frac{\partial w}{\partial \xi} + \frac{1}{\rho}\frac{\partial p}{\partial \xi}\tilde{z} = 0, \\ \frac{1}{L}\frac{\partial \rho}{\partial \tau} + (u\tilde{x} + v\tilde{y} + w\tilde{z})\frac{\partial \rho}{\partial \xi} + (\tilde{x}\frac{\partial u}{\partial \xi} + \tilde{y}\frac{\partial v}{\partial \xi} + \tilde{z}\frac{\partial w}{\partial \xi})\rho = 0, \\ \frac{1}{L}\frac{\partial \rho_i}{\partial \tau} + (u\tilde{x} + v\tilde{y} + w\tilde{z})\frac{\partial \rho_i}{\partial \xi} + (\tilde{x}\frac{\partial u}{\partial \xi} + \tilde{y}\frac{\partial v}{\partial \xi} + \tilde{z}\frac{\partial w}{\partial \xi})\rho_i = 0. \end{cases} \tag{44}$$

The system (44) can be written in the matrix form of (20), where $\mathbf{A}$, $(4 + N) \times (4 + N)$, is given by:

$$\mathbf{A} = \begin{pmatrix} 0 & \beta\tilde{x} & \beta\tilde{y} & \beta\tilde{z} & 0 & 0 & \dots & 0 \\ \frac{1}{\rho}\tilde{x} & \lambda_0 & 0 & 0 & 0 & 0 & \dots & 0 \\ \frac{1}{\rho}\tilde{y} & 0 & \lambda_0 & 0 & 0 & 0 & \dots & 0 \\ \frac{1}{\rho}\tilde{z} & 0 & 0 & \lambda_0 & 0 & 0 & \dots & 0 \\ 0 & \tilde{x}\rho & \tilde{y}\rho & \tilde{z}\rho & \lambda_0 & 0 & \dots & 0 \\ 0 & \tilde{x}\rho_1 & \tilde{y}\rho_1 & \tilde{z}\rho_1 & 0 & \lambda_0 & \dots & 0 \\ . & . & . & . & . & . & \dots & . \\ 0 & \tilde{x}\rho_{N-1} & \tilde{y}\rho_{N-1} & \tilde{z}\rho_{N-1} & 0 & 0 & \dots & \lambda_0 \end{pmatrix}. \tag{45}$$

The columns and rows 6 to $N+4$ correspond to the species densities. The matrix $\mathbf{A}$ has $N+2$ eigenvalues $\lambda_0 = u\tilde{x} + v\tilde{y} + w\tilde{z}$, and the eigenvalues $\lambda_1 = 1/2(\lambda_0 + s)$ and $\lambda_2 = 1/2(\lambda_0 - s)$, where $s = \sqrt{\lambda_0^2 + 4\frac{\beta}{\rho}}$ is the artificial speed of sound.

Applying the Riemann method [50] for the system (44) we obtain

$$\begin{cases} \frac{a}{\beta}(\tilde{p} - p_l) + b(\tilde{u} - u_l) + c(\tilde{v} - v_l) + d(\tilde{w} - w_l) + e(\tilde{\rho} - \rho_l) + \sum_{i=1}^{N-1} f_i(\tilde{\rho}_i - \rho_{il}) = 0, \\ -a\frac{\rho}{\beta}\lambda_l + b\tilde{x} + c\tilde{y} + d\tilde{z} = 0, \\ a\tilde{x} + b(\lambda_0 - \lambda_l) + e\rho\tilde{x} + \sum_{i=1}^{N-1} f_i\rho_i\tilde{x} = 0, \\ a\tilde{y} + c(\lambda_0 - \lambda_l) + e\rho\tilde{y} + \sum_{i=1}^{N-1} f_i\rho_i\tilde{y} = 0, \\ a\tilde{z} + d(\lambda_0 - \lambda_l) + e\rho\tilde{z} + \sum_{i=1}^{N-1} f_i\rho_i\tilde{z} = 0, \\ e(\lambda_0 - \lambda_l) = 0, \\ f_i(\lambda_0 - \lambda_l) = 0, \\ i = 1,\ N-1, \end{cases} \tag{46}$$

where the subscript l stands for the characteristics. For $\lambda = \lambda_0$, (46) yields

$$\begin{cases} \frac{a}{\beta}(\tilde{p} - p_0) + b(\tilde{u} - u_0) + c(\tilde{v} - v_0) + d(\tilde{w} - w_0) + e(\tilde{\rho} - \rho_0) + \sum_{i=1}^{N-1} f_i(\tilde{\rho}_i - \rho_{i0}) = 0, \\ -a\frac{\rho}{\beta}\lambda_0 + b\tilde{x} + c\tilde{y} + d\tilde{z} = 0, \\ a\tilde{x} + e\rho\tilde{x} + \sum_{i=1}^{N-1} f_i\rho_i\tilde{x} = 0, \\ a\tilde{y} + e\rho\tilde{y} + \sum_{i=1}^{N-1} f_i\rho_i\tilde{y} = 0, \\ a\tilde{z} + e\rho\tilde{z} + \sum_{i=1}^{N-1} f_i\rho_i\tilde{z} = 0, \\ e \cdot 0 = 0, \\ f_i \cdot 0 = 0, \\ i = 1,\ N-1. \end{cases} \tag{47}$$

From the above system we obtain

$$a = \frac{\beta}{\lambda_0\rho}(b\tilde{x} + c\tilde{y} + d\tilde{z}) \tag{48}$$

and

$$e = -a\frac{1}{\rho} - \sum_{i=1}^{N-1} f_i\frac{\rho_i}{\rho} = -\frac{\beta}{\lambda_0\rho}(b\tilde{x} + c\tilde{y} + d\tilde{z}) - \sum_{i=1}^{N-1} f_i\frac{\rho_i}{\rho}. \tag{49}$$

Substituting the formulas for a and e into the first equation of the system (47), we obtain:

$$\left((\tilde{p}-p_0)\frac{1}{\lambda_0\rho}\tilde{x}-b\frac{\beta}{\lambda_0\rho^2}\tilde{x}(\tilde{\rho}-\rho_0)+(\tilde{u}-u_0)\right)b+\left((\tilde{p}-p_0)\frac{1}{\lambda_0\rho}\tilde{y}-\frac{\beta}{\lambda_0\rho^2}y(\tilde{\rho}-\rho_0)+(\tilde{v}-v_0)\right)c$$
$$+\left((\tilde{p}-p_0)\frac{1}{\lambda_0\rho}\tilde{z}-b\frac{\beta}{\lambda_0\rho^2}\tilde{z}(\tilde{\rho}-\rho_0)+(\tilde{w}-w_0)\right)d+\sum_{i=1}^{N-1}f_i\left((\tilde{\rho}_i-\rho_{i0})-\frac{\rho_i}{\rho}(\tilde{\rho}-\rho_0)\right)=0. \tag{50}$$

For a non-trivial solution of (50), the terms in the brackets should be zero, thus

$$\begin{cases}\frac{(\tilde{p}-p_0)}{\lambda_0\rho}\tilde{x}-\frac{\beta(\tilde{\rho}-\rho_0)}{\lambda_0\rho^2}\tilde{x}+(\tilde{u}-u_0)=0,\\ \frac{(\tilde{p}-p_0)}{\lambda_0\rho}\tilde{y}-\frac{\beta(\tilde{\rho}-\rho_0)}{\lambda_0\rho^2}\tilde{y}+(\tilde{v}-v_0)=0,\\ \frac{(\tilde{p}-p_0)}{\lambda_0\rho}\tilde{z}-\frac{\beta(\tilde{\rho}-\rho_0)}{\lambda_0\rho^2}\tilde{z}+(\tilde{w}-w_0)=0,\\ (\tilde{\rho}_i-\rho_{i0})-\frac{\rho_i}{\rho}(\tilde{\rho}-\rho_0)=0,\\ i=1,\ N-1.\end{cases} \tag{51}$$

For $\lambda=\lambda_1=(\lambda_0+s)/2$ one can write $\lambda_0-\lambda_1=\lambda_2$. This yields,

$$\begin{cases}\frac{a}{\beta}(\tilde{p}-p_1)+b(\tilde{u}-u_1)+c(\tilde{v}-v_1)+d(\tilde{w}-w_1)+e(\tilde{\rho}-\rho_1)+\sum_{i=1}^{N-1}f_i(\tilde{\rho}_i-\rho_{i1})=0,\\ -a\frac{\rho}{\beta}\lambda_1+b\tilde{x}+c\tilde{y}+d\tilde{z}=0,\\ a\tilde{x}+b\lambda_2+e\rho\tilde{x}+\sum_{i=1}^{N-1}f_i\rho_i\tilde{x}=0,\\ a\tilde{y}+c\lambda_2+e\rho\tilde{y}+\sum_{i=1}^{N-1}f_i\rho_i\tilde{y}=0,\\ a\tilde{z}+d\lambda_2+e\rho\tilde{z}+\sum_{i=1}^{N-1}f_i\rho_i\tilde{z}=0,\\ e\lambda_2=0,\\ f_i\lambda_2=0,\\ i=1,\ N-1.\end{cases} \tag{52}$$

From the last two equations, we obtain $e=0$ and $f_i=0$, thus yielding:

$$\begin{cases}a\frac{1}{\beta}(\tilde{p}-p_1)+b(\tilde{u}-u_1)+c(\tilde{v}-v_1)+d(\tilde{w}-w_1)=0,\\ -a\frac{\rho}{\beta}\lambda_1+b\tilde{x}+c\tilde{y}+d\tilde{z}=0,\\ -\frac{\tilde{x}}{\lambda_2}a=b,\\ -\frac{\tilde{y}}{\lambda_2}a=c,\\ -\frac{\tilde{z}}{\lambda_2}a=d.\end{cases} \tag{53}$$

Multiplying the last three equations by $\tilde{x}$, $\tilde{y}$ and $\tilde{z}$, respectively, and taking into account that $\tilde{x}^2+\tilde{y}^2+\tilde{z}^2=1$ and $\lambda_1\lambda_2=-\frac{\beta}{\rho}$, the second equation in (53) becomes an identity. Substituting the formulas for the coefficients b, c and d into the first equation of (53) we obtain

$$a\left(\frac{1}{\beta}(\tilde{p}-p_1)-\frac{\tilde{x}}{\lambda_2}(\tilde{u}-u_1)-\frac{\tilde{y}}{\lambda_2}(\tilde{v}-v_1)-\frac{\tilde{z}}{\lambda_2}(\tilde{w}-w_1)\right)=0, \tag{54}$$

which yields that either we have a solution identical to zero for all the coefficients or

$$\frac{1}{\beta}(\tilde{p}-p_1)-\frac{\tilde{x}}{\lambda_2}(\tilde{u}-u_1)-\frac{\tilde{y}}{\lambda_2}(\tilde{v}-v_1)-\frac{\tilde{z}}{\lambda_2}(\tilde{w}-w_1)=0. \tag{55}$$

Because $\lambda_2\lambda_1=-\frac{\beta}{\rho}$, (55) can be written as

$$(\tilde{p}-p_1)+\lambda_1\rho(\tilde{x}(\tilde{u}-u_1)-\tilde{y}(\tilde{v}-v_1)-\tilde{z}(\tilde{w}-w_1))=0. \tag{56}$$

Similarly, when $\lambda=\lambda_2=(\lambda_0-s)/2$ and $\lambda_0-\lambda_2=\lambda_1$, we obtain

$$(\tilde{p}-p_2)+\lambda_2\rho(\tilde{x}(\tilde{u}-u_2)-\tilde{y}(\tilde{v}-v_2)-\tilde{z}(\tilde{w}-w_2))=0. \tag{57}$$

The solution of (51), (56) and (57) yields the following formulas for the characteristics-based variables,

$$\begin{cases}\tilde{p}=\frac{1}{s}(\lambda_1 p_2-\lambda_2 p_1-\beta(R_1-R_2)),\\ \tilde{u}=u_0+\frac{\tilde{x}}{s\rho}R_3,\\ \tilde{v}=v_0+\frac{\tilde{y}}{s\rho}R_3,\\ \tilde{w}=v_0+\frac{\tilde{z}}{s\rho}R_3,\\ \tilde{\rho}=\rho_0+\frac{\rho}{\beta}\left(p-p_0+\frac{\lambda_0}{s}R_3\right),\\ \tilde{\rho}_i=\rho_{i0}+\frac{\rho_i}{\beta}\left(p-p_0+\frac{\lambda_0}{s}R_3\right),\end{cases} \tag{58}$$

where the auxiliary functions R_1, R_2 and R_3 are defined by (31). The eigenvalues obtained for the *conservative* scheme are the same with those obtained for the *hybrid* scheme; these correspond to the eigenvalues obtained by other researchers for variable density flow equations [39,41,51]. The formulas for pressure and velocities are the same with those obtained for the hybrid scheme. The density formulas for the three schemes are different: compare the last two equations in (30), (43) and (58). For the *conservative* scheme the density formulas include a pseudo-compressibility term. Numerical experiments presented in Part II of this study reveal that the addition of the pseudo-compressibility term increases the speed of propagation of density disturbances, which in turn leads to faster convergence both in steady and time-dependent flows.

3.4. Intercell variables interpolation

For the calculation of the characteristics flow variables $\mathbf{V}_l=(p_l,u_l,v_l,w_l,\rho_l,\rho_{i,l})^{\mathrm{T}}$ $(l=0,1,2)$, at the cell faces we employ Godunov-type discretization. Note that λ_1 and λ_2 are always positive and negative, respectively, thus obtaining

$$\begin{cases}\mathbf{V}_0=\frac{\mathbf{V}_\mathrm{L}+\mathbf{V}_\mathrm{R}}{2}-\mathrm{sign}(\lambda_0)\frac{\mathbf{V}_\mathrm{R}-\mathbf{V}_\mathrm{L}}{2},\\ \mathbf{V}_1=\mathbf{V}_\mathrm{L},\\ \mathbf{V}_2=\mathbf{V}_\mathrm{R},\end{cases} \tag{59}$$

where $\mathrm{sign}(\lambda_0)=1$ or -1 for $\lambda_0>0$ and $\lambda_0<0$, respectively. The variables with indices 'L' and 'R' denote left and right states of intercell values that are calculated by polynomial interpolation.

Different versions of first, second and higher-order interpolation schemes can be found in [14]. In Appendix A we present the derivation of different orders of interpolation including first-order,

$$\mathbf{V}_{\mathrm{L},j+1/2}=\mathbf{V}_j,\quad \mathbf{V}_{\mathrm{R},j+1/2}=\mathbf{V}_{j+1}, \tag{60}$$

second-order

$$\begin{cases}\mathbf{V}_{\mathrm{L},j+1/2}=\frac{3}{2}\mathbf{V}_j-\frac{1}{2}\mathbf{V}_{j-1},\\ \mathbf{V}_{\mathrm{R},j+1/2}=\frac{3}{2}\mathbf{V}_{j+1}-\frac{1}{2}\mathbf{V}_{j+2},\end{cases} \tag{61}$$

and third-order,

$$\begin{cases} \mathbf{V}_{\mathrm{L},j+1/2} = \frac{5}{6}\mathbf{V}_j - \frac{1}{6}\mathbf{V}_{j-1} + \frac{1}{3}\mathbf{V}_{j+1}, \\ \mathbf{V}_{\mathrm{R},j+1/2} = \frac{5}{6}\mathbf{V}_{j+1} - \frac{1}{6}\mathbf{V}_{j+2} + \frac{1}{3}\mathbf{V}_j. \end{cases} \tag{62}$$

For problems encompassing sharp interfaces such as Rayleigh–Taylor instabilities, flux limiting versions of the intercell interpolation can be employed. For further discussion on flux limiters we refer the reader to [14]. Finally, we mention that the viscous fluxes in (11) are discretized by second-order central differences.

3.5. Summary of advective flux calculation

The numerical steps for the calculation of the advective flux are summarized below:

Step 1: Calculate the eigenvalues λ_l for $l = 0,1,2$ using the velocities u, v and w from the previous time step.
Step 2: Use (59) in conjunction with first, second or third-order interpolation to calculate the left and right states of the characteristics variables. For each eigenvalue, we calculate one set of primitive variables along the characteristics.
Step 3: Use formulas (30), (43) or (58) – depending on the choice of the scheme – to calculate the reconstructed characteristics-based variables.
Step 4: Use the characteristics-based (tilde) variables to calculate the advective flux at the cell faces of the control volume.

The above four steps are performed for the calculation of the advective fluxes in ξ, η and ζ directions. Then, the discretized flux derivatives are added (including the viscous fluxes in the case of the Navier–Stokes equations) and the system of equations is iterated in time using a time integration scheme. In this study, we use a fourth-order Runge–Kutta scheme which is presented in Section 4.

4. Time integration

The system of equations is solved in pseudo-time for each real-time step. This is achieved by using a fourth-order Runge–Kutta scheme [56] in conjunction with a nonlinear multigrid method [55]. The fourth-order Runge–Kutta scheme is written as

$$\begin{aligned} \mathbf{U}_1 &= \mathbf{U}_n, \\ \mathbf{U}_2 &= \mathbf{U}_n - \frac{\Delta\tau}{2}\mathrm{RHS}(\mathbf{U}_1), \\ \mathbf{U}_3 &= \mathbf{U}_n - \frac{\Delta\tau}{2}\mathrm{RHS}(\mathbf{U}_2), \\ \mathbf{U}_4 &= \mathbf{U}_n - \Delta\tau\mathrm{RHS}(\mathbf{U}_3), \\ \mathbf{U}_{n+1} &= \mathbf{U}_n - \frac{\Delta\tau}{6}(\mathrm{RHS}(\mathbf{U}_1) + 2\mathrm{RHS}(\mathbf{U}_2) + 2\mathrm{RHS}(\mathbf{U}_3) + \mathrm{RHS}(\mathbf{U}_4)), \end{aligned} \tag{63}$$

where RHS represents the right-hand side of the Navier–Stokes operator in (11). The time step on each Runge–Kutta iteration is locally defined according to the convergence requirements of the advective part of the Navier–Stokes equations. However, for flows at low Reynolds or Peclet numbers the pseudo-time

step should be restricted for stability purposes. Therefore, it is defined locally according to the convergence requirements of inviscid, viscous and diffusion parts of the Navier–Stokes equations:

$$\begin{cases} \Delta\tau_{i,j,k} = \min\left(\Delta\tau^{\text{inv}}_{i,j,k}, \Delta\tau^{\text{vis}}_{i,j,k}, \Delta\tau^{\text{diff}}_{i,j,k}\right), \\ \Delta\tau^{\text{inv}}_{i,j,k} = \frac{\text{CFL}_{\text{inv}}}{(\max_{m=1-6}\{(|\lambda_1|,|\lambda_2|)\}_m)_{i,j,k}}, \\ \Delta\tau^{\text{vis}}_{i,j,k} = \frac{\text{CFL}_{\text{vis}}Re}{4(\max_{n=1,2,3}(\mathrm{d}l_n))_{i,j,k}}, \\ \Delta\tau^{\text{diff}}_{i,j,k} = \frac{\text{CFL}_{\text{vis}}Pe}{4(\max_{n=1,2,3}(\mathrm{d}l_n))_{i,j,k}}, \end{cases} \tag{64}$$

where $\mathrm{d}l_n$ denotes the computational cell dimension in the three directions $n = \xi, \eta, \zeta$ and m stands for the index of the cell face.

5. Constant density limit

In this section, we examine (30), (43) and (58) in the limit of constant-density incompressible flows. We remind that the formulas for constant-density, incompressible flow [14,36] are given by

$$\tilde{\mathbf{U}} = \begin{pmatrix} \tilde{p} \\ \tilde{u} \\ \tilde{v} \\ \tilde{w} \end{pmatrix} = \begin{pmatrix} \frac{1}{2s}(\lambda_1 k_2 - \lambda_2 k_1) \\ R\tilde{x} + u_0(\tilde{y}^2 + \tilde{z}^2) - v_0\tilde{x}\tilde{y} - w_0\tilde{x}\tilde{z} \\ R\tilde{y} + v_0(\tilde{x}^2 + \tilde{z}^2) - w_0\tilde{z}\tilde{y} - u_0\tilde{x}\tilde{y} \\ R\tilde{z} + w_0(\tilde{y}^2 + \tilde{x}^2) - v_0\tilde{z}\tilde{y} - u_0\tilde{x}\tilde{z} \end{pmatrix}, \tag{65}$$

where

$$R = \frac{1}{2s}[p_1 - p_2 + \tilde{x}(\lambda_1 u_1 - \lambda_2 u_2) + \tilde{y}(\lambda_1 v_1 - \lambda_2 v_2) + \tilde{z}(\lambda_1 w_1 - \lambda_2 w_2)], \tag{66}$$

$$k_1 = p_1 + \lambda_1(u_1\tilde{x} + v_1\tilde{y} + w_1\tilde{z}), \tag{67}$$

$$k_2 = p_2 + \lambda_2(u_2\tilde{x} + v_2\tilde{y} + w_2\tilde{z}). \tag{68}$$

We consider first the transport CB scheme. Setting density equal to one,[1] the formula (30) and the corresponding eigenvalues are written as

$$\begin{cases} p = \frac{1}{2s}(\lambda_1 p_2 - \lambda_2 p_1 - \beta(R_1 - R_2)), \\ u = u_0 + \frac{\tilde{x}}{2s}R_3, \\ v = v_0 + \frac{\tilde{y}}{2s}R_3, \\ w = w_0 + \frac{\tilde{z}}{2s}R_3, \\ \lambda_{0,1,2} = \lambda_0, \lambda_0 \pm \sqrt{\lambda_0^2 + \beta}. \end{cases} \tag{69}$$

Using $\lambda_1\lambda_2 = -\beta$, we can modify the formula for pressure as follows:

$$\begin{aligned} p &= \frac{1}{2s}(\lambda_1 p_2 - \lambda_2 p_1) + \frac{\lambda_1\lambda_2}{2s}(\tilde{x}(u_2 - u_1) + \tilde{y}(v_2 - v_1) + \tilde{z}(w_2 - w_1)) \\ &= \frac{1}{2s}(\lambda_1(p_2 + \lambda_2(\tilde{x}u_2 + \tilde{y}v_2 + \tilde{z}w_2)) - \lambda_2(p_1 + \lambda_1(\tilde{x}u_1 + \tilde{y}v_1 + \tilde{z}w_1))), \end{aligned} \tag{70}$$

[1] Always working with dimensionless variables, thus for constant density flows the dimensionless density would be equal to one.

which is exactly the same as for the incompressible, constant-density case [14,36]. Similarly, for the u velocity we obtain

$$u = u_0 + \tilde{x}R + \frac{\tilde{x}}{2s}(\lambda_2 - \lambda_1)(\tilde{x}u_0 + \tilde{y}v_0 + \tilde{z}w_0) = \tilde{x}R - (1+\tilde{x}^2)u_0 - \tilde{x}\tilde{y}v_0 - \tilde{x}\tilde{z}w_0$$
$$= \tilde{x}R + (\tilde{y}^2 + \tilde{z}^2)u_0 - \tilde{x}\tilde{y}v_0 - \tilde{x}\tilde{z}w_0, \tag{71}$$

where the auxiliary function R is given by (66). Eq. (71) is the same as for the incompressible, constant-density case (65). The results for the other two velocity components can be obtained in a similar fashion. In the constant density limit the characteristics-based solutions for the *hybrid* (43) and *conservative* (58) CB schemes *become identical*, therefore, it is sufficient to present the analysis only for one of these formulations. Let us consider the variables for the *conservative* CB scheme (58) and set density equal to one in the formulas for pressure, velocities and eigenvalues,

$$\begin{cases} \tilde{p} = \frac{1}{s}(\lambda_1 p_2 - \lambda_2 p_1 - \beta(R_1 - R_2)), \\ \tilde{u} = u_0 + \frac{\tilde{x}}{s}R_3, \\ \tilde{v} = v_0 + \frac{\tilde{y}}{s}R_3, \\ \tilde{w} = v_0 + \frac{\tilde{z}}{s}R_3, \\ \lambda_{0,1,2} = \lambda_0, \frac{\lambda_0 \pm \sqrt{\lambda_0^2 + 4\beta}}{2}. \end{cases} \tag{72}$$

Defining $\lambda_1^* = 2\lambda_1$, $\lambda_2^* = 2\lambda_2$ and $\beta^* = 4\beta$, (72) are written as

$$\begin{cases} \tilde{p} = \frac{1}{2s}\left(\lambda_1^* p_2 - \lambda_2^* p_1 - \frac{\beta^*}{2}(R_1 - R_2)\right), \\ \tilde{u} = u_0 + \frac{\tilde{x}}{2s}R_3, \\ \tilde{v} = v_0 + \frac{\tilde{y}}{2s}R_3, \\ \tilde{w} = v_0 + \frac{\tilde{z}}{2s}R_3, \\ \lambda_0, \lambda_{1,2}^* = \lambda_0, \quad \lambda_0 \pm \sqrt{\lambda_0^2 + \beta^*}, \end{cases} \tag{73}$$

where $s = \sqrt{\lambda_0^2 + \beta^*}$ and $\lambda_{1,2}^* = \lambda_0 \pm s$. The pressure and eigenvalues in (73) cannot be brought into the form (65). Thus, (73) provides a new characteristics-based scheme for constant-density incompressible flows. At this stage, it is interesting to examine the numerical behavior of the *conservative* and *transport* schemes for constant-density incompressible flows. Computations were performed for the flow through a sudden expansion–contraction. The problem has been previously studied both computationally and experimentally [52,53]. Experiments [52] and previous simulations [53,54] have shown that depending on the Reynolds number the flow through a sudden expansion–contraction may exhibit symmetric or asymmetric flow separation. We have carried out computations for two Reynolds numbers, $Re = 30$ and $Re = 116$ that correspond to symmetric and asymmetric separation, respectively (Fig. 3). The computational grid contained 37×37 and 237×109 points in the small channels and main section, respectively. To measure the difference in the results between the variants of the schemes, the maximum of the pressure difference, throughout the flow field, p_{diff}, was used

$$p_{\text{diff}} = \max_{i,j} \left| \frac{p_{i,j}^{\text{cons}} - p_{i,j}^{\text{trans}}}{p_{i,j}^{\text{trans}}} \right| \times 100, \tag{74}$$

where the 'cons' and 'trans' denote the conservative and transport variants; the latter is identical to the original characteristics-based scheme when the density is considered constant. The computations revealed that the difference in the results between the *conservative* variant and the original constant-density version of the scheme do not exceed 0.06% and 0.07% for symmetric and asymmetric cases, respectively.

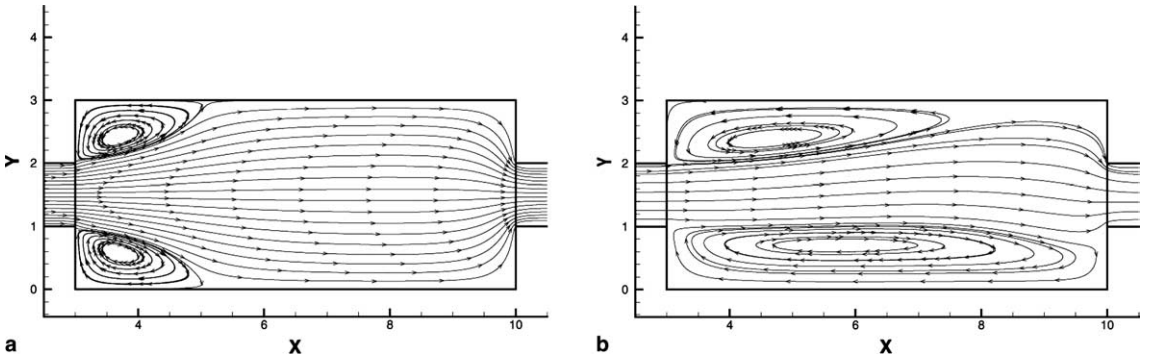

Fig. 3. Computational results for the flow through a sudden expansion–contraction ($Re = 30$) and ($Re = 116$). The differences in the results between *transport* and *conservative* schemes do not exceed 0.07%. The hybrid and conservative schemes become identical for constant density flows. (a) $Re = 30$, (b) $Re = 116$.

Table 1
Number of multigrid cycles required to achieve reduction of the residuals by four orders of magnitude for the computations of the incompressible (constant-density) flow through a sudden expansion–contraction

	$Re = 30$	$Re = 116$
Transport scheme	33	68
Hybrid/conservative scheme	26	49

However, the transport and conservative formulations exhibit some differences in the convergence. Table 1 shows the number of multigrid cycles required to achieve four orders of magnitude reduction of the residuals for the transport and conservative schemes.[2] This fact motivated a detailed investigation of the multigrid convergence of characteristics-based schemes for variable-density incompressible flows (see Part II of this study).

6. Conclusions

To date the artificial compressibility formulation has received scant attention in connection with the simulation of variable-density incompressible flows. In this paper, we presented the derivation of characteristics-based schemes for variable-density incompressible flows in the framework of artificial-compressibility formulation. We have shown that artificial compressibility results in three different numerical formulations, which subsequently lead to three variants of characteristics-based schemes.

The *transport* scheme uses the divergence-free condition in the (total) density transport equation. The *conservative* scheme uses the equations in a fully conservative form. In the *hybrid* scheme the conservative equation for the total density is used to eliminate the density variable from the momentum equations, while similar to the *transport* variant, the divergence-free condition is employed to simplify the species transport equations. The above formulations result in different characteristics-based schemes. With regard to the density field, the *transport* and *hybrid* schemes lead to reconstruction of species densities along the streamlines, whereas the *conservative* scheme leads to a reconstruction formula that contains pseudo-compressibility

[2] The hybrid scheme becomes identical the conservative scheme in the constant-density limit.

terms. Moreover, the *transport* scheme differs from the *conservative* and *hybrid* schemes with respect to pressure and velocity formulas.

The numerical behavior of the schemes was examined in the limit of constant density incompressible flows. It was shown that the reconstruction formulas for the *transport* scheme become the same with the corresponding ones for the characteristics-based scheme for constant-density incompressible flows.For constant density flows the formulas for the *hybrid* and *conservative* schemes become identical. They, however, differ with regard to the original formulas obtained for constant-density incompressible flow. In effect, the constant-density limit of *hybrid/conservative* scheme can also be considered as a new version of the characteristics-based scheme for constant density flows. With regard to the behavior of the schemes in the limit of constant-density flows, numerical experiments were carried out showing that both hybrid/conservative and transport schemes provide the same accuracy but differ in terms of convergence (measured here by the number of multigrid cycles). The multigrid implementation of the above methods as well as detailed studies to assess their accuracy and efficiency in steady and unsteady variable-density flows are presented in [57].

Acknowledgements

The financial support from the UK's Engineering and Physical Sciences Research Council (GR/S13668) is greatly acknowledged.

Appendix A

Consider the one-dimensional stencil (equidistant grid in the computational space) and define two states, left and right, for the intercell variables, as follows

$$\mathbf{V}_{\mathrm{L},j+1/2} = a\mathbf{V}_j - b\mathbf{V}_{j-1} + c\mathbf{V}_{j+1} + d\mathbf{V}_{j+2} \tag{75}$$

for the left state, and

$$\mathbf{V}_{\mathrm{R},j+1/2} = a\mathbf{V}_{j+1} - b\mathbf{V}_{j+2} + c\mathbf{V}_j + d\mathbf{V}_{j-1} \tag{76}$$

for the right state. The coefficients a, b, c and d are determined according to the following procedure:

The derivative of the characteristic variable at the cell center for the case of a positive eigenvalue – the result will be analogous if a negative eigenvalue is considered – yields

$$\begin{aligned}\left(\frac{\partial \mathbf{V}}{\partial \xi}\right)_j &= \mathbf{V}_{\mathrm{L},j+1/2} - \mathbf{V}_{\mathrm{L},j-1/2} = a\mathbf{V}_j - b\mathbf{V}_{j-1} + c\mathbf{V}_{j+1} + d\mathbf{V}_{j+2} \\ &= (a\mathbf{V}_{j-1} - b\mathbf{V}_{j-2} + c\mathbf{V}_j + d\mathbf{V}_{j+1})(a-c)\mathbf{V}_j - (a+b)\mathbf{V}_{j-1} + b\mathbf{V}_{j-2} + (c-d)\mathbf{V}_{j+1} + d\mathbf{V}_{j+2}.\end{aligned} \tag{77}$$

By developing all variables in a Taylor series expansion around the cell center j, (77) yields

$$\begin{aligned}\left(\frac{\partial \mathbf{V}}{\partial \xi}\right)_j &= (a-c)\mathbf{V}_j - (a+b)[\mathbf{V}_j - \mathbf{V}^{(1)} + \mathbf{V}^{(2)} - \mathbf{V}^{(3)} + \mathbf{V}^{(4)}] + b[\mathbf{V}_j - 2\mathbf{V}^{(1)} + 4\mathbf{V}^{(2)} - 8\mathbf{V}^{(3)} + 16\mathbf{V}^{(4)}] \\ &\quad + (c-d)[\mathbf{V}_j + \mathbf{V}^{(1)} + \mathbf{V}^{(2)} + \mathbf{V}^{(3)} + \mathbf{V}^{(4)}] + d[\mathbf{V}_j + 2\mathbf{V}^{(1)} + 4\mathbf{V}^{(2)} + 8\mathbf{V}^{(3)} + 16\mathbf{V}^{(4)}],\end{aligned} \tag{78}$$

where the superscripts denote order of derivatives and the denominators in the Taylor series expansion have been omitted and can be considered to be part of the unknown coefficients which are yet to be determined; the grid spacing is considered to be equal to one since we are working in the computational space. Eq. (78) is written as

$$\left(\frac{\partial \mathbf{V}}{\partial \xi}\right)_j = (a-b+c+d)\mathbf{V}^{(1)} + [c-a+3(b+d)]\mathbf{V}^{(2)} + [c+a+7(d-b)]\mathbf{V}^{(3)} + [c-a+15(b+d)]\mathbf{V}^{(4)}. \tag{79}$$

Using (79) schemes of different order of accuracy can be derived.

- First-order upwind scheme for

$$a = 1 \quad \text{and} \quad b = c = d = 0. \tag{80}$$

The left and right states of the variables at the cell face are accordingly defined by

$$\mathbf{V}_{\mathrm{L},j+1/2} = \mathbf{V}_j, \quad \mathbf{V}_{\mathrm{R},j+1/2} = \mathbf{V}_{j+1}. \tag{81}$$

- The second-order scheme is obtained for $c = d = 0$,

$$a - b = 1, \tag{82}$$

for satisfying the CFL like restriction, i.e., having the coefficient of the first-order derivative equal to one, and

$$3b - a = 0, \tag{83}$$

for eliminating the second-order derivative term from (79). From (82) and (83) the values $a = 3/2$ and $b = 1/2$ are obtained. The left and right states are accordingly defined by

$$\begin{cases} \mathbf{V}_{\mathrm{L},j+1/2} = \frac{3}{2}\mathbf{V}_j - \frac{1}{2}\mathbf{V}_{j-1}, \\ \mathbf{V}_{\mathrm{R},j+1/2} = \frac{3}{2}\mathbf{V}_{j+1} - \frac{1}{2}\mathbf{V}_{j+2}. \end{cases} \tag{84}$$

- The third-order scheme is obtained for $d = 0$, the CFL-like restriction

$$a - b + c = 1, \tag{85}$$

and the following conditions for eliminating the second- and third-order derivative terms from (79)

$$\begin{cases} 3b - a + c = 0, \\ a - 7b + c = 0. \end{cases} \tag{86}$$

Eqs. (85) and (86) give the values $a = 5/6$, $b = 1/6$ and $c = 1/3$. The left and right states are accordingly defined

$$\begin{cases} \mathbf{V}_{\mathrm{L},j+1/2} = \frac{5}{6}\mathbf{V}_j - \frac{1}{6}\mathbf{V}_{j-1} + \frac{1}{3}\mathbf{V}_{j+1}, \\ \mathbf{V}_{\mathrm{R},j+1/2} = \frac{5}{6}\mathbf{V}_{j+1} - \frac{1}{6}\mathbf{V}_{j+2} + \frac{1}{3}\mathbf{V}_j. \end{cases} \tag{87}$$

References

[1] B.H. Weigl, P. Yager, Microfluidic diffusion-based separation and detection, Science 15 (1999) 346.
[2] W.E. TeGrotenhuis, R. Cameron, M.G. Butcher, P.M. Martin, R.S. Wegeng, Micro Channel Devices for Efficient Contacting of Liquids in Solvent Extraction, Separation Science and Technology, PNNL-SA-28743, 1998.
[3] R.F. Ismagilov, A.D. Stock, P.J.A. Kenis, G. Whitesides, Experimental and theoretical scaling laws for transverse diffusive broadening in two-phase laminar flows in microchannels, Appl. Phys. 76 (17) (2000) 2376.
[4] K.B. Greiner, M. Deshpande, J.R. Gilbert, R.F. Ismagilov, A.D. Stroock, G.M. Whitesides, Design Analysis and 3D Measurement of Diffusive Broadening in a Y-Mixer', Technical Proceedings of Micro Total Analysis Systems, Enschede, The Netherlands, MicroTAS, 2000, pp. 87–90.

[5] A.E. Kamholtz, P. Yager, Theoretical analysis of molecular diffusion in pressure-driven laminar flow in microfluidic channels, Biophys. J. 80 (2001) 155.
[6] P. Chassaing, R.A. Antonia, F. Anselmet, L. Joly, S. Sarkar, Variable Density Fluid Turbulence, Kluwer Academic, Dordrecht, 2002.
[7] R.B. Pember, L.H. Howell, J.B. Bell, P. Colella, W.Y. Cruchfield, W.A. Fiveland, J.P. Jessee, An adaptive projection method for unsteady, low-Mach number combustion, Combust. Sci. Technol. 140 (1998) 123.
[8] P.K. Wong, Y.-K. Lee, C.-M. Ho, Deformation of DNA molecules by hydrodynamic focusing, J. Fluid Mech. 497 (2003) 55.
[9] P.G Baines, Topographic Effects in Stratified Flows, Cambridge University Press, Cambridge, MA, 1998.
[10] S.B. Dalziel, P.F. Linden, D.L. Youngs, Self-similarity and internal structure of turbulence induced by Rayleigh–Taylor instability, J. Fluid Mech. 399 (1999) 1.
[11] D.L. Lindl, R.L. McCrory, E.M. Campbell, Progress toward ignition and burn propagation in inertial confinement fusion, Physics Today 32–40 (1992).
[12] W.D. Arnett, J.N. Bahcall, R.P. Kirshner, S.E. Woosley, Supernova 1987A, Ann. Rev. Astron. Astrophys. 27 (1987) 629.
[13] R. Scardovelli, S. Zaleski, Direct numerical simulation of free-surface and interfacial flow, Ann. Rev. Fluid Mech. 31 (1999) 567.
[14] D. Drikakis, W. Rider, High-resolution Methods for Incompressible and Low-speed Flows, Springer, Berlin, 2004.
[15] E.G. Puckett, A.S. Almgren, J.B. Bell, D.L. Marcus, W.J. Rider, A high-order projection method for tracking fluid interfaces in variable density incompressible flows, J. Comput. Phys. 130 (1997) 269.
[16] E.F. Toro, Shock-capturing Methods for Shallow Flows, John Wiley and Sons, New York, 2001.
[17] S.O. Unverdi, G. Tryggvason, Computations of multi-fluid flows, Physica D 60 (1992) 70.
[18] G. Tryggvason, A. Fernandez, A. Esmaeeli, B. Bunner, Direct numerical simulations of multiphase flows, in: D. Drikakis, B.J. Geurts (Eds.), Turbulent Flow Computation, Kluwer Academic, Dordrecht, 2002.
[19] J.B. Bell, P. Colella, H.M. Glaz, A Second-order projection method of the incompressible Navier–Stokes equations, J. Comp. Phys. 85 (1989) 257.
[20] J.B. Bell, D.L. Marcus, A second-order projection method for variable-density flows, J. Comp. Phys. 101 (1992) 334.
[21] A.S. Almgren, J.B. Bell, W.G. Szymczak, A numerical method for the incompressible Navier–Stokes equations based on an approximate projection, SIAM J. Sci. Comput. 17 (2) (1996) 358.
[22] A.S. Almgren, J.B. Bell, P. Colella, L.H. Howell, M.L. Welcome, A conservative projection method for the variable-density incompressible Navier–Stokes equations, J. Comp. Phys. 142 (1998) 1.
[23] W.J. Rider, D.B. Kothe, E.G. Puckett, I.D. Aleinov, Accurate and robust methods for variable density incompressible flows with discontinuities, in: V. Venkatakrishnan, M.D. Salas, S.R. Chakravarthy (Eds.), Barriers and Challenges in Computational Fluid Dynamics, Kluwer Academic Publishers, Boston, MA, 1998, ISBN 0-7923-4855-9, pp. 213–230.
[24] J.-L. Guermond, L. Quartapelle, A projection FEM for variable density incompressible flows, J. Comp. Phys. 165 (2000) 167.
[25] Y. Fraigneau, J.-L. Guermond, L. Quartapelle, Approximation of variable density incompressible flows by means of finite elements and finite volumes, Commun. Numer. Methods Eng. 17 (2001) 893.
[26] A.J. Chorin, A numerical method for solving incompressible viscous flow problems, J. Comput. Phys. 2 (1967) 12.
[27] D. Pan, S.R. Chakravarthy, Unified formulation for incompressible flows, AIAA Paper 89-0122, 1989
[28] D. Kwak, J.L.C. Chang, S.P. Shanks, S.R. Chakravarthy, A three-dimensional incompressible Navier–Stokes flow solver using primitive variables, AIAA J. 24 (3) (1986) 390.
[29] P.-M. Hartwich, C.-H. Hsu, C.H. Liu, Vectorizable implicit algorithms for the flux difference split, Three-dimensional Navier–Stokes equations, J. Fluids Eng. 110 (1) (1988) 297.
[30] C.L. Merkle, M. Athavale, Time accurate unsteady incompressible flow algorithms based on artificial compressibility, AIAA Paper 87-1137, 1987
[31] W.Y. Soh, J.W. Goodrich, Unsteady solution of incompressible Navier–Stokes equations, J. Comput. Phys. 79 (1988) 113.
[32] S.E. Rogers, D. Kwak, Upwind differencing scheme for the time-accurate incompressible Navier–Stokes equations, AIAA J. 28 (2) (1990) 253.
[33] S.E. Rogers, D. Kwak, C. Kiris, Steady and unsteady solutions of the incompressible Navier–Stokes equations, AIAA J. 29 (4) (1991) 603.
[34] M. Breuer, D. Hänel, A dual time-stepping method for 3-D viscous incompressible vortex flows, Comput. Fluids 22 (1993) 467.
[35] W.-W. Kim, S. Menon, An unsteady incompressible Navier–Stokes solver for large Eddy simulation of turbulent flows, Int. J. Numer. Methods Fluids 31 (1999) 983.
[36] D. Drikakis, P.A. Govatsos, D.E. Papatonis, A characteristic-based method for incompressible flows, Int. J. Numer. Methods Fluids 19 (1994) 667.
[37] D. Drikakis, Embedded turbulence model in numerical methods for hyperbolic conservation laws, Int. J. Numer. Methods Fluids 39 (2002) 763.
[38] D. Drikakis, Numerical issues in very large eddy simulation, CD-ROM Proceedings of ECCOMAS CFD, Swansea, UK, 2001.
[39] U. Riedel, Finite-volume scheme on unstructured grids for stiff chemically reacting flows, Combust. Sci. Technol. 135 (1998) 99.

[40] Dartzi Pan, Chih-Hao Chang, The capturing of free surfaces in incompressible multi-fluid flows, Int. J. Numer. Methods Fluids 33 (2) (2000) 203.
[41] L. Qian, D.M. Gauson, D.M. Ingram, C.G. Mingham, Cartesian cut-cell two-fluid solver for hydraulic flow problems, J. Hydr. Eng. 129 (2003) 689.
[42] A. Eberle, Characteristic flux averaging approach to the solution of Euler's equations, VKI Lecture Series, Computational Fluid Dynamics 1987-04, 1987.
[43] G.K. Batchelor, An Introduction to Fluid Dynamics, Cambridge University Press, Cambridge, MA, 1967.
[44] P. Wesseling, Principles of Computational Fluid Dynamics, Springer, Berlin-Heidelberg, 2000.
[45] W. Wangard III, D.S. Dandy, B.J. Miller, A numerically stable method for integration of the multicomponent species diffusion equations, J. Comput. Phys. 174 (1) (2001) 460.
[46] V. Vesovic, Predicting viscosity of natural gas, 14th Symposium on Thermophysical Properties, Boulder, Colorado, June 25–30, 2000.
[47] S. Bastea, Transport properties of fluid mixtures at high pressures and temperature. Application to the detonation products of HMX, 12th International Detonation Symposium, Wyndham San Diego at Emerald Plaza, August 11–16, 2002.
[48] E.L. Cussler, Diffusion, Mass Transfer in Fluid Systems, Cambridge University Press, New York, 1984.
[49] E.L. Cussler, Multicomponent Diffusion, Elsevier, Amsterdam, 1976.
[50] R. Courant, D. Hilbert, Methods of Mathematical Physics, John Wiley & Sons Inc, New York, 1991.
[51] E. Dick, Flux-vector splitting method for steady Navier–Stokes equations, Int. J. Numer. Methods Fluids 8 (1988) 317.
[52] J. Mizushima, H. Okamoto, H. Yamaguchi, Stability of flow in a channel with a suddenly expanded part, Phys. Fluids 8 (11) (1996) 2933.
[53] J. Mizushima, Y. Shiotani, Transitions and instabilities of flow in a symmetric channel with a suddenly expanded and contracted part, J. Fluid Mech. 434 (2001) 355.
[54] S. Patel, D. Drikakis, Prediction of flow instabilities and transition using high-resolution methods, Int. J. Num. Meth. Fluids (in print); also European Congress on Computational Methods in Applied Sciences and Engineering Conference (ECCOMAS), Jyvaskyla, Filand, 24–28 July 2004
[55] D. Drikakis, O.P. Iliev, D.P. Vassileva, A nonlinear multigrid method for the three-dimensional incompressible Navier–Stokes equations, J. Comput. Phys. 146 (1998) 301.
[56] C.-W. Shu, S. Osher, Efficient implementation of essentially non-oscillatory shock capturing schemes, J. Comput. Phys. 77 (1988) 439.
[57] E. Shapiro, D. Drikakis, Artificial compressibility, characteristics-based schemes for variable density, incompressible, multi-species flows. Part 2. Multigrid implementation and numerical tests, J. Comput. Physics 210 (2005) 608–631.